Geotextiles and Geomembranes 46 (2018) 402–413

Contents lists available at ScienceDirect

Geotextiles and Geomembranes

journal homepage: www.elsevier.com/locate/geotexmem

Back-analysis of geotechnical parameters on PVD-improved ground in the Mekong Delta

H. Hiep, S.G. Chung*

Dept. of Civil Engineering, Dong-A University, 37, #550 Street, Nakdong-ro 550, Busan, 49315, Republic of Korea

ARTICLE INFO

Keywords:
Geosynthetics
Clay
Field monitoring
Back analysis
FEA

ABSTRACT

This study presents a back-analysis of geotechnical parameters on prefabricated vertical drain improved ground at a site in the Mekong Delta. Various time – settlement behaviors that reflected different clay thicknesses and loading patterns were observed. The total surface settlement behavior at several monitoring locations was simulated using an updated exponential method that considered staged construction. The analyzed results were validated by substituting the values into a theoretical solution for radial consolidation. The estimated theoretical behaviors were comparable with the monitored behaviors. The geotechnical parameters were back-analyzed by applying the previously analyzed results to various theoretical and empirical formulas. However, the use of extensometer data that were installed at large intervals produced different values of the geotechnical properties. Furthermore, finite element analysis supported the back-analyzed total settlement behaviors and nearly disregarded the application of the geotechnical properties that were obtained using either surface or subsurface settlement data. However, settlements and excess pore pressures in the sublayers were not successfully predicted even when the geotechnical properties were adjusted. Thus, subsurface instruments that can be installed closely in thick clay deposits are required to reliably reevaluate the variations in geotechnical properties along a certain depth.

1. Introduction

Ground improvement of thick clay deposits has been conducted to develop marginal lands in many parts of the world. Prefabricated vertical drain (PVD) techniques are among the most extensively used ground improvement methods. A key issue in PVD techniques is whether field monitoring (e.g., settlement and excess pore pressure behaviors from the initial settlement to the ultimate settlement) and behavior prediction are reliably conducted. Despite numerous studies conducted over the past two or more decades, the precise prediction of consolidation and delayed (long-term) settlements, along with their rates, remains difficult (Bergado et al., 2002; Chu et al., 2006; Indraratna et al., 2012; Jang and Chung, 2014; Karim et al., 2011; Liu and Chu, 2009; Lo et al., 2008; Olsen, 1998; Rowe and Taechakumthorn, 2008; Rujikiatkamjorn and Indraratna, 2015; Saowapakpiboon et al., 2011; Taechakumthorn and Rowe, 2012; Watabe and Leroueil, 2015). The underestimation of settlement and consolidation time have been reported in several projects, such as the Changi Airport project in Singapore (Bo et al., 2003) and the Noksan reclamation project in Korea (Chung, 1999). An unreliable prediction may be related to various factors, including the limitations of the theoretical solutions, evaluated soil, and PVD-related parameters, the construction procedure, deterioration of the installed PVDs. Thus, feedback is essentially used to improve the prediction of settlement behaviors.

Several observational methods can be used to predict the ultimate settlement and the settlement rate (Asaoka, 1978; Debats et al., 2013; Tan et al., 1991; Chung et al., 2014b) and the results can be applied to reevaluate geotechnical parameters (Bergado et al., 1992; Bartlett and Alcorn, 2004; Cao et al., 2001; Chung et al., 2009, 2014b; Chung and Lee, 2010; Leroueil et al., 1990; Magnan et al., 1983; Voottipruex et al., 2014). Numerical analysis is also adopted for similar purposes (Bergado et al., 1993, 1996; Cao et al., 2001; Chai et al., 2001, 2011; Hawlader et al., 2002). Observational methods can easily evaluate the average geotechnical parameters. However, their variations along certain depths are difficult to reflect, whereas numerical analysis exhibits an opposite trend. Back-analyzed geotechnical properties are generally used to compare laboratory and field soil test results and to predict the settlement behaviors of neighboring sites. However, whether the results obtained from observational and numerical methods are comparable with each other is rarely verified (Lam et al., 2015; Rezania et al., 2017). Thus, the two approaches should be simultaneously applied to

* Corresponding author.
E-mail addresses: hiepportcoast@gmail.com (H. Hiep), sgchung@dau.ac.kr (S.G. Chung).

https://doi.org/10.1016/j.geotexmem.2018.03.005
Received 27 May 2017; Received in revised form 6 March 2018; Accepted 10 March 2018

validate the appropriateness of the back-analyzed geotechnical properties.

This study aims to reliably reevaluate the geotechnical properties and to predict the settlement behaviors of a PVD-improved ground in the Mekong Delta, in which the effect of the poorly adopted sampling techniques are compensated. The effects of different thicknesses and stepped loadings on the monitored settlements and excess pore pressures were investigated. An observational method (i.e., the exponential model) was modified to consider the effect of staged construction on the settlement. Various geotechnical properties were determined based on the back-analyzed results. Furthermore, the estimated properties were compared with the laboratory and field test results. Moreover, finite element (FE) analysis was performed using the estimated geotechnical parameters, and the analysis results were compared with the two previous results. Further considerations to improve the back-analysis process were discussed based on the comparison.

2. Observational methods and determination of geotechnical properties

2.1. Observational methods

2.1.1. End of the primary consolidation settlement

The graphical method of Asaoka (1978) is known to produce the most reliable value of the ultimate (ρ_{ult}) or the end of the primary consolidation settlement (ρ_{100}). The ultimate settlement is graphically determined from a special diagram that is plotted using each settlement read out at time interval (Δt) on the ρ-t curve.

$$\rho_{ult} = \frac{\beta_0}{1-\beta_1} \tag{1}$$

where β_0 and β_1 are the intercept and slope of a straight line in the special diagram, respectively. However, ρ_{ult} (or ρ_{100}) in this method varies depending on the selected time interval (Arulrajah et al., 2004; Asaoka, 1978; Chung et al., 2014b; Edil et al., 1991). The ultimate settlement is also estimated using the hyperbolic relationship of ρ-t, as follows (Tan et al., 1991):

$$\rho = \frac{t}{\alpha + \beta t} \tag{2a}$$

$$\lim_{t\to\infty}\rho = \lim_{t\to\infty}\frac{1}{\alpha/t+\beta} = \rho_{ult} = \frac{1}{\beta} \tag{2b}$$

The hyperbolic methods overestimate the ultimate value, which depends on the percentage of data (Chung et al., 2014a, b).

Recently, an exponential model is used as a rational method to simulate consolidation behavior (Chung et al., 2014b).

$$\rho = \rho_{ult}[1-\exp(-\eta t)]^{\kappa} \tag{3}$$

where three unknowns (ρ_{ult}, η, and κ) are determined by best fitting the measured data. The data after the end of construction are generally used in observational methods. However, the current study considers stepped loading data as part of the primary consolidation settlement. Thus, the time (t_0) to initiate the primary consolidation in the monitored ρ-t relationships is determined as follows. Eq. (3) is rearranged to consider the initial settlement and time.

$$-\ln\left(1-\left(\frac{\rho}{\rho_{100}}\right)^{1/\kappa}\right) = \eta\,(t-t_0) \tag{4}$$

where the unknowns (ρ_{100}, η, and κ) are successfully obtained using Excel Solver.

2.1.2. Consolidation coefficient

For thick deposits with small drain spacing, only radial flow may be approximately considered to occur, thereby neglecting the effect of vertical flow (Lee and Chung, 2010). That is,

$$U_h = \left[1-\exp\left(-\frac{8}{F}T_h\right)\right] \tag{5a}$$

or

$$U_h = \left[1-\exp\left(-\frac{8}{F_n}T_{h(n)}\right)\right] \tag{5b}$$

where T_h ($=c_h t/d_e^2$) and $T_{h(n)}$ ($=c_{h(n)}t/d_e^2$) are the time factors; d_e is the diameter of the influence zone of each drain; F is a factor that accounts for the combined effects of spacing ($F_n \approx \ln(n) - 0.75$ for $n > 10$), [$F_s = (k_h/k_s - 1)\ln(s)$] is the smear; ($F_r$) is the well resistance; $n = d_e/d_w$, in which d_w is the equivalent diameter of the drain; $s = d_s/d_w$, in which d_s is the equivalent diameter of the smear zone; and k_h and k_s are the coefficients of the horizontal permeability of the undisturbed soil and smear zone, respectively. Thus, a relation is obtained based on Eq. (6) as follows:

$$\frac{c_h}{F} = \frac{c_{h(n)}}{F_n} = \frac{c_{h(n+s)}}{F_{n+s}} \tag{6}$$

where $c_{h(n+s)}$ is the consolidation coefficient that corresponds to F_{n+s}. The radial consolidation coefficient $c_{h(n)}$ for the ideal condition (without the effects of smear and well resistance) can be obtained with a given F_n.

Magnan et al. (1983) proposed a method for estimating the $c_{h(n)}$ of PVD-improved ground based on the analytical solution developed by Asaoka (1978).

$$c_{h(n)} = \frac{d_e^2}{8}\frac{F_n}{\Delta t}\cdot\ln\beta_1 \tag{7}$$

Chung et al. (2009) presented a method for estimating $c_{h(n)}$ based on the hyperbolic method.

$$c_{h(n)} = [0.1333\ln(n) - 0.0906]\cdot\frac{\beta d_e^2}{\alpha} \tag{8}$$

$c_{h(n)}$ that varies with time can be considered with the exponential model (Chung et al., 2014b). That is, the following expression is derived from Eqs. (3) and (5b):

$$c_{h(n)-var} = \frac{T_{h(n)}}{t}d_e^2 = \frac{\eta F_n d_e^2}{8}\frac{\ln(1-U_h)}{\ln(1-U_{exp}^{1/\kappa})} = \frac{\eta\, d_e^2}{8}\cdot[\ln(n)-0.75]\cdot\Phi \tag{9}$$

where $\Phi = \ln(1-U_h)/\ln(1-U_{exp}{}^{1/\kappa})$ and $U_{exp} = \rho/\rho_{100} = U_h$. The Φ value rapidly decreases at the initial part and then gradually decreases with increasing U_h. Thus, the average value of Φ is determined for $30\% \le U_h \le 90\%$ as follows:

$$\Phi_{ave} = \frac{\int \Phi dU}{\int dU} = [0.971\kappa^{-0.119} + 0.028\kappa^{-1.978}]^{\,5.123} \tag{10}$$

where the coefficient of determination $r^2 = 0.9999$. Thus, the average value of $c_{h(n)}$ is obtained by

$$c_{h(n),ave} = \frac{\eta\, d_e^2}{8}\cdot[\ln(n)-0.75]\cdot\Phi_{ave} \tag{11}$$

where Φ_{ave} approximately corresponds to Φ at $U_h = 60\%$.

2.2. Determination of geotechnical properties

2.2.1. Compressive parameters

Compressive parameters may be estimated using the applied load, the monitored settlement, and excess pore pressure. Recompression and consolidation settlements for the 1D condition are calculated as follows:

$$\rho_r = \sum_{i=1}^{m}\frac{C_{Si}}{1+e_{0i}}\Delta h_i\log\left(\frac{\sigma'_{pi}}{\sigma'_{v0i}}\right), \tag{12a}$$

$$\rho_c = \sum_{i=1}^{m} \frac{C_{Ci}}{1 + e_{0i}} \Delta h_i \log\left(\frac{\sigma'_{v0i} + \Delta\sigma_i}{\sigma'_{pi}}\right) \quad (12b)$$

where ρ_r and ρ_c are the recompression and virgin compression, respectively; e_0 is the in situ void ratio; σ'_{v0} is the effective overburden stress; i is the number of layers; and σ'_p is the preconsolidation stress. The stress increment $\Delta\sigma$ is considered for the initial and final loading conditions (Leroueil et al., 1990).

$$\Delta\sigma_{(initial)} = \gamma_r H_{cr} \quad (13a)$$

$$\Delta\sigma_{(final)} = \gamma_r H_{cr} + \Delta\gamma(\rho + h_w) - 0.5\gamma_w\rho \quad (13b)$$

where γ_r and H_{cr} are the unit weight and the critical height of the fill, respectively; $\Delta\gamma$ is the difference between the saturated and bulk unit weights; h_w is the incremental water height caused by fill placement; and γ_w is the unit weight of water.

The recompression (C_r) and compression (C_c) indexes are generally correlated with e_0 as follows:

$$C_r = a_1 + b_1 e_o \quad (14a)$$

$$C_c = a_2 + b_2 e_o \quad (14b)$$

where a_1, a_2, b_1, and b_2 are constants. Thus, C_r and C_c can be back-analyzed using Eqs. (12) and (14), respectively.

The preconsolidation stress σ'_p should be determined using the incremental stress and dissipated excess pore pressure.

$$\sigma'_p = \sigma'_{v0} + \Delta\sigma_{cr} - \Delta u \quad (15)$$

where $\Delta\sigma_{cr}$ and Δu are the incremental stress and the excess pore pressure induced by the critical fill height H_{cr}, respectively. When piezometers are not closely installed, the variation in σ'_p along the depth is insufficiently obtained.

2.2.2. Coefficient of permeability

This section presents a method for estimating the coefficient of radial permeability under an ideal condition. The coefficient of horizontal permeability $k_{h0\text{-diss}}$ is obtained using the piezocone dissipation tests as follows (Baligh and Levadoux, 1986):

$$k_{h0-diss} = \frac{\gamma_w}{2.3\sigma'_{v0}} RR \cdot c_{h(OC)-diss} \quad (16)$$

where RR is the recompression ratio ($0.005 < RR < 0.02$, with an average value of 0.01), and $c_{h(OC)\text{-diss}}$ is the coefficient of radial consolidation obtained from the piezocone dissipation test on intact clay. Similarly, values may be expressed using the reevaluated RR ($= C_r/(1 + e_0)$) or CR ($= C_c/(1 + e_0)$) values.

$$k_{h0-back} = \frac{\gamma_w}{2.3\sigma'_{v0}} RR \cdot c_{h(OC)-diss}, \text{ or } \frac{\gamma_w}{2.3\sigma'_{v0}} CR \cdot c_{h(NC)-diss} \quad (17)$$

where $c_{h(OC)}/c_{h(NC)} = CR/RR$. Thus, the difference between the $c_{h(n)}$ and $c_{h(NC)\text{-diss}}$ can be expressed by the ratio of the respective areas as follows:

$$R_c = \frac{\int c_{h(NC)-diss}\, dz}{\int c_{h(n)} dz} \quad (18)$$

where $R_c = F/F_n$. Subsequently, the coefficient of permeability $k_{h0(n)}$ for the ideal condition may be adjusted to obtain the same $k_{h0\text{-back}}$ as follows:

$$k_{h0(n)} = \frac{k_{h0-back}}{R_c} \quad (19)$$

3. Reclamation work

3.1. Site description

A reclamation site is located beside the Soai Rap River and at the south gateway of Ho Chi Minh City, Vietnam (Fig. 1). A terminal port called “Saigon Premier Container Terminal” was constructed at the site. The area of the site is approximately 46,500 m^2, and the container berth has a length of 949 m for a vessel of 50,000 DWT. A total of 21 and 17 boreholes were drilled for the basic and detailed design, respectively. Undisturbed samples were taken using the Osterberg piston and Shelby samplers with a 2 m interval. A total of 44 piezocone tests (CPTU) were conducted after placing a sand fill of 0.8–1.6 m. The field vane (FV) test, which is a double-rod type with a blade that measures 13 cm high and 6.5 cm wide, was conducted in 21 locations. Conventional oedometer tests with a duration of 24 h and a stress increment ratio of 1.0 were conducted.

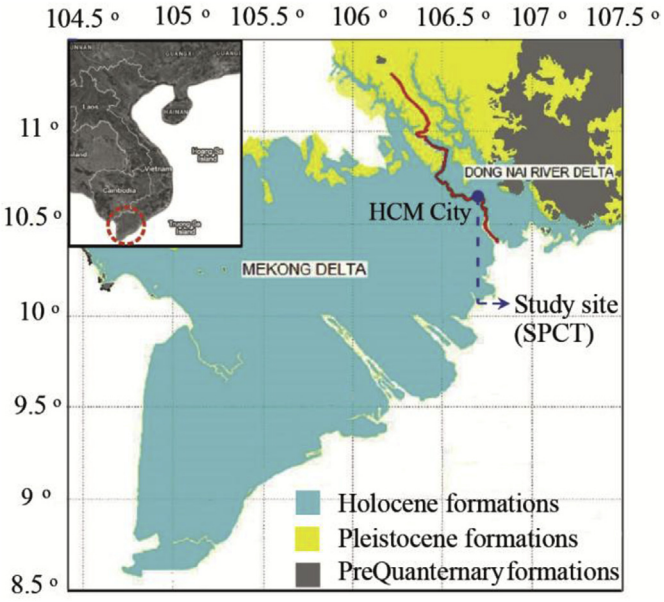

Fig. 1. Location.

The deposit consisted of upper Holocene clay (very soft to soft) and lower Pleistocene clay (stiff to very stiff). In addition, a thin sand layer was occasionally intercepted between the two types of clay (Nguyen et al., 2000; Ta et al., 2002). The water level was directly affected by a tidal variation of approximately 3.5 m a day in the Soai Rap River. The thickness of the upper clay (approximately 1000–5000 years BP), which was normally consolidated based on geological history (Nguyen et al., 2005), varied from 9 to 40 m. Fig. 2 shows a typical soil profile, which consists of three main soil layers: (i) the upper layer (0–35 m) with three sublayers [1a – very soft clay (MH–CH, 0–11 m), 1b – very soft to soft clay (MH–CH, 11–20 m), and 1c – soft to medium clay (CH, 20–35 m)]; (ii) sandy soil layer (30–35 m); and (iii) stiff clay (below 35 m). The total unit weight (γ_t), water content (w_n), and in situ void ratio (e_0) varied consistently with depth. The liquid and plastic limits were relatively constant (w_L = 70%–80% and w_P = 35%–38%). The w_n values were higher than those of w_L along the entire depth (i.e., liquidity index $I_L > 1.0$), which indicated that the clay was cemented (or structured). The compression indexes were widely distributed: C_{c1} = 0.5–1.6 and C_{c2} = 0.1–0.6 for the initial and second virgin compressions, respectively. The preconsolidation stresses (σ'_p) were approximately 1.3–3.5 times higher than the effective overburden stress σ'_{v0}. The field vane strength ($s_{u,FV}$) increased linearly with depth, which exhibited a wide variation. The corrected cone resistance (q_t) and pore pressure (u_2) tended to increase linearly with an increase in depth, which appeared to be governed dominantly by σ'_{v0}.

3.2. Ground improvement with PVD

For the reclamation, the vegetation and organic layers (1.0–2.0 m

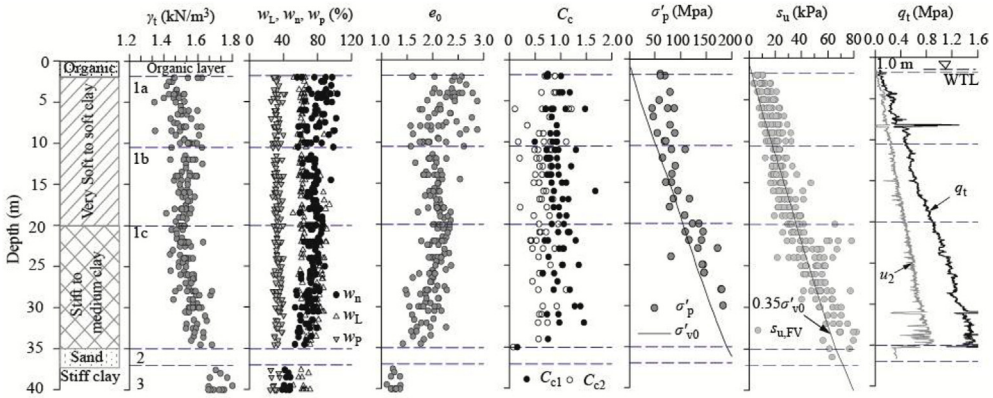

Fig. 2. Basic soil properties at the study site.

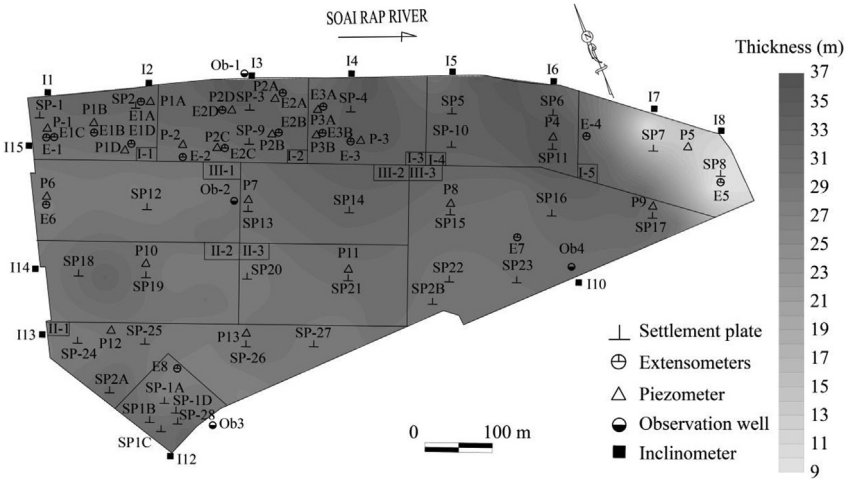

Fig. 3. Filed instrumentation and thickness of soft clay.

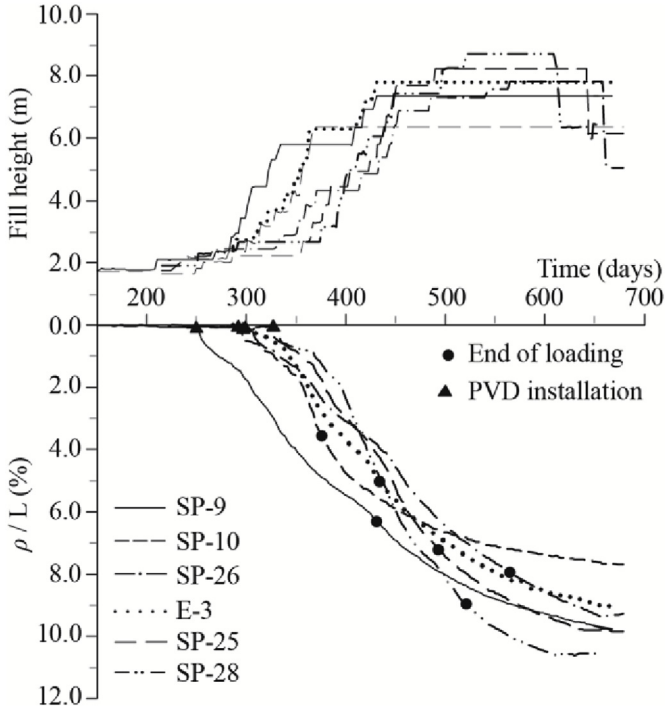

Fig. 4. Construction schedules and time – settlement plots.

thick) were initially removed. Thereafter, the sand fill of 1.6–2.2 m was placed. A detailed site investigation was conducted and various instruments were installed. Preloading with PVD was applied to improve the ground. The sequence of the reclamation work is summarized as follows: (i) a sand blanket with a thickness of 0.5–0.8 m was placed, (ii) PVDs with a triangular pattern were installed up to a depth of 30–35 m with 1.5 m spacing; (iii) several types of instruments were installed, and (iv) fill construction to a height of 6.0–8.0 m was staged. The PVD, called Flodrain (FD4-EX), measures 4 mm × 100 mm and has a polypropylene nonwoven-type filter and a studded-type core. The PVD was installed using a hydraulic-type rig with a 60 mm × 120 mm rectangular-type mandrel and steel anchor plates.

After the surcharge, the shoulders of the embankment (toward the river bank) were stabilized by using soil – cement deep mixing columns. The fill materials, which were mostly sand, were obtained from adjacent provinces using waterway vehicles in the Soai Rap River. The transported materials were dumped and graded by bulldozers. The fill placement rate was 25–50 cm/week. The average bulk density of the fill material was approximately 1.9 kN/m^3.

3.3. Field monitoring and results

Fig. 3 shows the installed instruments. In particular, 28 settlement plates, 13 piezometers, 8 extensometers, 15 inclinometers, and 3 observational wells were installed. The piezometers were the vibrating wire type with a 13.3 cm-long tip. The magnetic-type extensometers and piezometers were installed at three levels in 13 locations. The inclinometers were installed along the river bank slope (toward the Soai Rap River). The observation wells, which comprised a perforated PVC

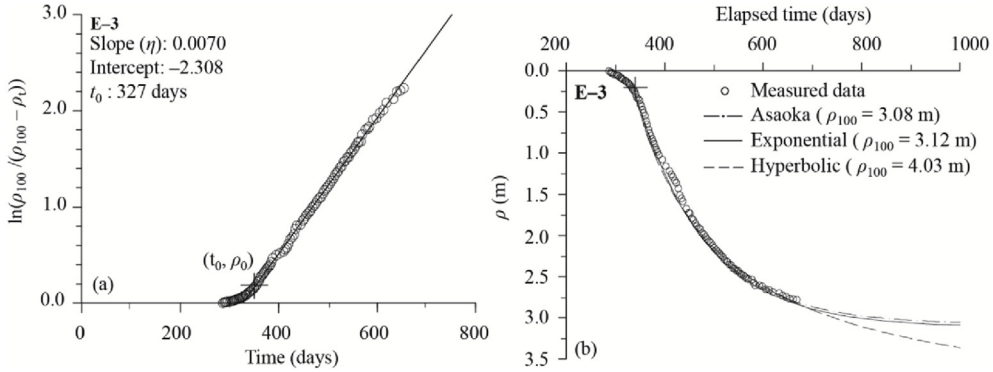

Fig. 5. Determination of the initial point of consolidation behaviors.

Table 1
Primary consolidation settlements obtained from three observational methods and strain rates.

Locations	L [a]	H [b]	H_{cr}	ρ_{100} (m)			ρ_m/ρ_{100} [d]	$\dot{\varepsilon}_f$ [e]
	(m)	(m)	(m)	Asaoka [c]	Hyperbolic	Exponential	(%)	($\times 10^{-8}$ s^{-1})
SP-9	33.3	7.38	2.97	3.50	4.40	3.48	94.15	5.46
SP-10	34.0	6.37	3.18	2.64	3.25	2.72	96.77	2.43
SP-25	33.6	8.25	3.32	3.59	4.66	3.70	91.50	1.72
SP-26	31.8	7.83	3.36	3.73	4.89	3.88	77.71	2.43
SP-28	31.8	8.72	3.19	3.81	5.01	3.93	87.05	1.82
E-3	34.0	8.03	3.84	3.08	4.03	3.12	89.29	2.88

[a] L = clay thickness.
[b] H = fill height.
[c] The time interval (Δt) used for Asaoka's method was 3 days.
[d] The ratio of the finally measured settlement (ρ_m) to the exponential method-based ρ_{100}.
[e] $\dot{\varepsilon}_f$ is the finally measured strain rate.

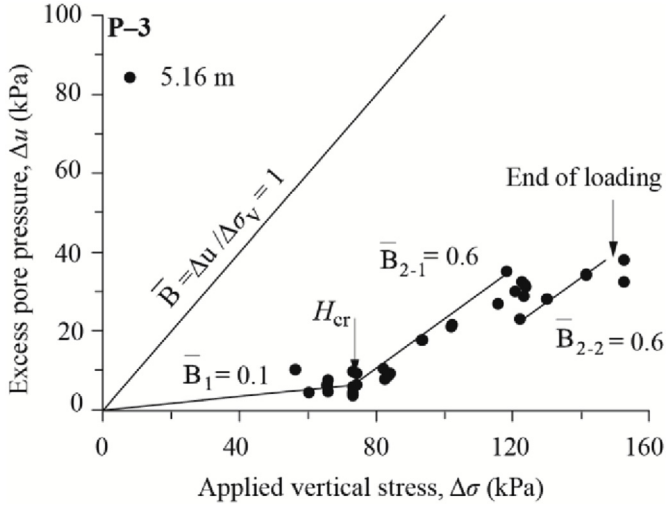

Fig. 6. Excess pore pressure versus applied load.

pipe with a 60 mm diameter, were installed at the boundary of the construction area and inside the embankments. Measurement frequency varied depending on the construction schedule, i.e., every 2-days during construction and twice a week after completion.

Fig. 4 shows the timelines of the construction and the normalized total settlements (ρ/L, where L is the thickness of the clay above the sand layer) at several sites, located in Zones I-1 to I-5 and II-2. The installation periods of the PVDs (200–260 days) and the fill placement rates (loading rates = 0.05–0.1 m/day during the period of 250–370 days and 420–440 days) differed at various monitoring points. A similar pattern of time – settlement relationships was approximately observed regardless of the locations and clay thicknesses as the fill placement was initiated. Abrupt changes in settlements occurred during PVD installation and end of construction.

4. Back-analysis and results

4.1. Consolidation behavior

Recompression was observed during the initial construction step (Fig. 4). Fig. 5a presents an example of an approach for graphically determining the initial values (ρ_0, t_0). Thus, the primary consolidation behavior can be simulated by substituting the measured data into Eq. (4) (Fig. 5b). Table 1 shows that H_{cr} = 2.97–3.84 m for a fill height of 6.37–8.72 m and L = 31–34 m. The ρ_{100} obtained using the exponential method was 0–3.5% higher than that obtained using the Asaoka method but was 20%–29% lower than that obtained using the hyperbolic method. This order is the same as those found in another case study (Chung et al., 2014b) and laboratory tests. The ratio of the final measured settlement to the predicted ρ_{100} (ρ_m/ρ_{100}) based on the results of the exponential method was 77.71%–96.67%. The strain rate at the final measured stage was approximately within the order of 10^{-8} s^{-1} at the final measured time. The strain rates are similar to the rates observed from the PVD-improved ground in Singapore (Cao et al., 2001).

4.2. σ'_p and compressive parameters

Fig. 6 shows a method for determining σ'_p using the field records for pore pressure (Leroueil et al., 1978, 1983; Morin et al., 1983). Stresses at the intersection between excess pore pressure increment (Δu) versus applied load increment ($\Delta\sigma_v$) were nearly identical to those associated with H_{cr}. Fig. 7a shows that the estimated σ'_p values were compared with the values obtained from the laboratory consolidation tests. The estimated σ'_p values were found within the upper bound of the tested values. The underestimation of σ'_p in the laboratory may be attributed

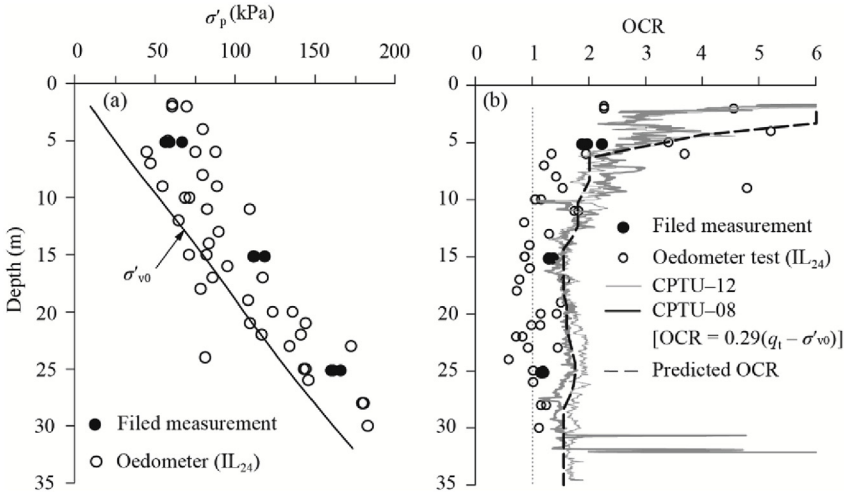

Fig. 7. Preconsolidation pressure.

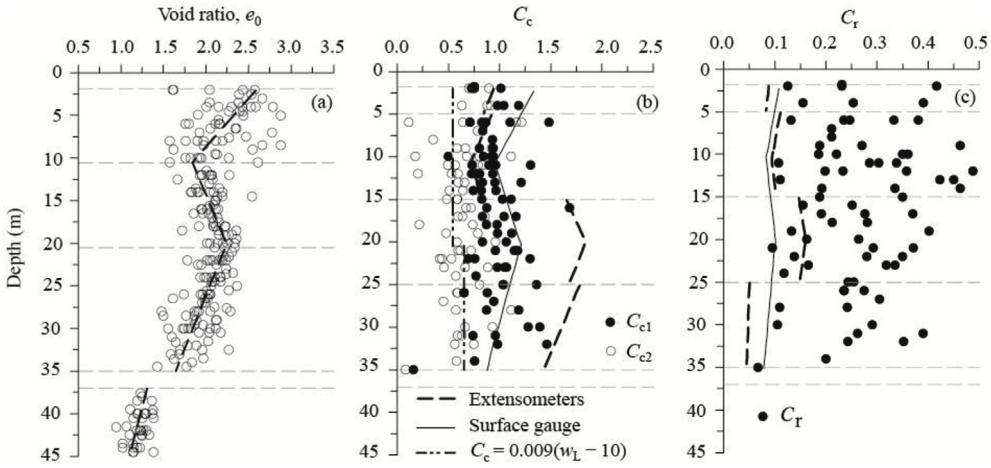

Fig. 8. Void ratio and back-analyzed compressive indexes at the E-3 location.

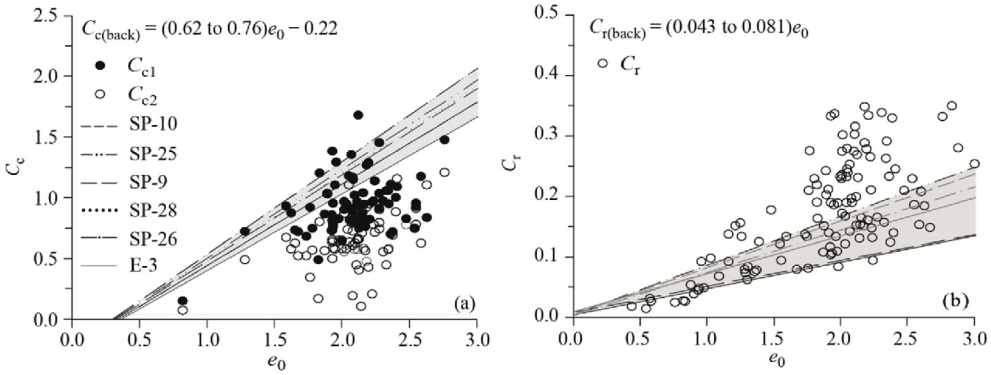

Fig. 9. C_c and C_r versus e_0.

to sample disturbance. Thus, the overconsolidation ratio ($OCR = \sigma'_p/\sigma'_{v0}$) was compared with the CPTU-based empirical formula, i.e., $OCR = \lambda(q_t - \sigma_{v0})/\sigma'_{v0}$. The prediction with $\lambda \approx 0.29$ was close to the measured values, which were less than $\lambda \approx 0.40$ for $OCR \leq 3$ (Singh and Chung, 2015) and $\lambda \approx 0.33$ for $OCR = 1$–40 (Kulhawy and Mayne, 1990). Consequently, the σ'_p values (represented by OCR) were assumed to be close to the CPTU-based and measured values (Fig. 7b).

w_n, γ_t, and e_0 varied consistently with depth (Fig. 2), which reflected geological history. Thus, the variation in e_0 according to each depositional unit was averagely determined (Fig. 8a). Then, C_c and C_r were estimated according to the variation in e_0 [Eqs. (12) and (14)], in which the thickness of each sublayer $\Delta H_i = 0.5$ m was selected (Fig. 9). For the six locations, the back-analyzed C_c ($= (0.62–0.76)e_0 - 0.22$) using the surface settlement data is found within the upper bound of C_{c1}, whereas C_r ($= (0.043–0.081)e_0$) is found within the lower bound of laboratory C_r values. The underestimation may also be attributed to sample disturbance. Fig. 8b and c shows that the C_c and C_r values in location E-3 that were estimated using extensometer data significantly differed from those obtained using surface settlement data. Moreover, the C_{c2} values obtained from the oedometer tests were nearly identical to those from a

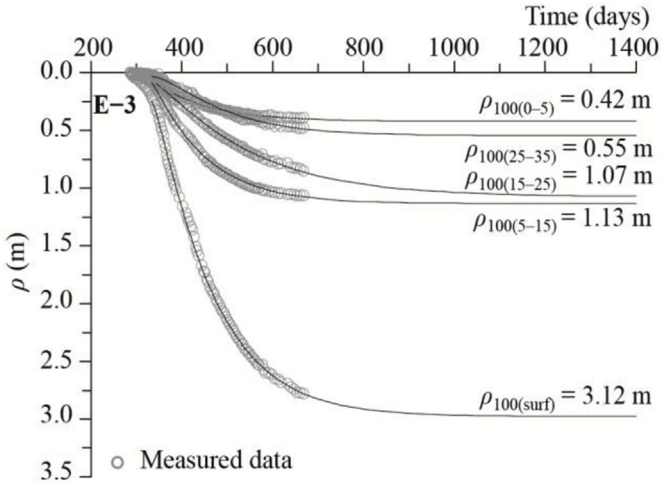

Fig. 10. Simulated curves with the back-analyzed $c_{h(n)}$ values (location E-3).

Table 2
Back-analyzed coefficients of consolidation.

Location	$\rho_{100} - \rho_0$	$c_{h(n)}$	$c_{h(n+s)}$	$c_{h(n)}$ from Asaoka	$c_{h(n)}$ from hyperbola
	(m)	(m^2/year)	(m^2/year)	(m^2/year)	(m^2/year)
E-3(surf)	2.902	1.775	2.591	1.924	1.995
E-3(0–5 m)	0.405	2.545	3.662	2.459	3.315
E-3(5–15 m)	1.050	2.139	3.077	2.419	3.054
E-3(15–25 m)	0.999	1.086	1.563	1.697	1.316
E-3(25–35 m)	0.518	1.266	1.822	2.143	1.712
SP-9	2.979	1.706	2.456	1.627	2.117
SP-10	2.420	2.836	5.360	2.981	3.466
SP-25	3.316	2.531	4.873	2.174	2.559
SP-26	3.347	2.103	2.559	1.363	1.424
SP-28	3.450	2.066	2.286	2.465	2.643

Note: k_h/k_s = 2.0 and d_s/d_m = 2.0; F_n = 2.42 and F_s = 1.06.

famous empirical equation (Skempton, 1944): $C_c = 0.009(w_L - 10)$. A similar result was observed from clay in Singapore, Bangkok, and Ariake (Tanaka, 2002). Accordingly, the back-analyzed C_{c1} based on the proposed method can be rationally used.

4.3. Consolidation and permeability coefficients

The consolidation behaviors for the location E-3 were simulated using the monitored ρ-*t* data with ρ_0 and ρ_{100} (or ρ_{ult}) (Fig. 10). η and κ were determined, and $c_{h(n)}$ was calculated using Eq. (11) as $c_{h(n)}$ = 1.09–2.55 m^2/year and $c_{h(n+s)}$ = 1.57–3.66 m^2/year. A similar analysis was conducted for the remaining six locations as $c_{h(n)}$ = 1.71–2.84 m^2/year and $c_{h(n+s)}$ = 2.29–5.36 m^2/year (Table 2). However, slightly and significantly different values of $c_{h(n)}$ were

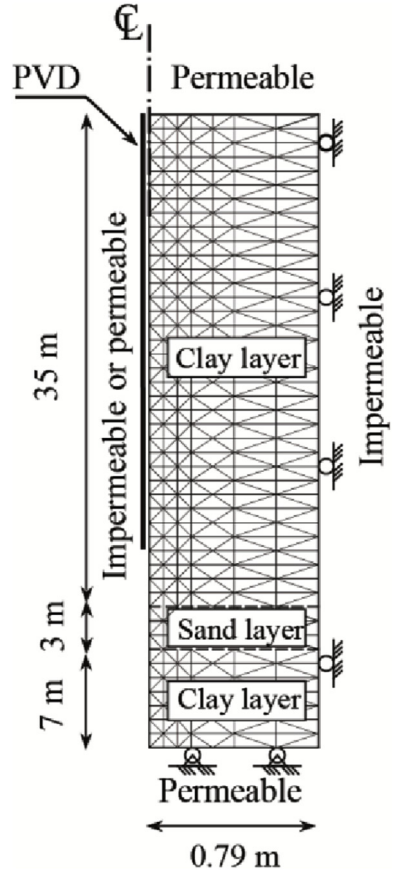

Fig. 12. Axisymmetric unit cell.

Table 3
Four FE analyses for location E-3.

Case	C_c and C_r (Fig. 8b and c)	k_{h0} (Fig. 11c)	R_c (= F/F_n = $c_h/c_{h(n)}$)
I	Constant (C_c = 1.05 and C_r = 0.095)	$k_{h0(n)-surf}$	1.45
II	Surface gauge-based varying values	$k_{h0(n)-surf}$	1.45
III	Extensometer-based values	$k_{h0(n)-ext}$	1.80
IV	Extensometer-based values	$k_{h0(n)-ext(mod)}$	1.47

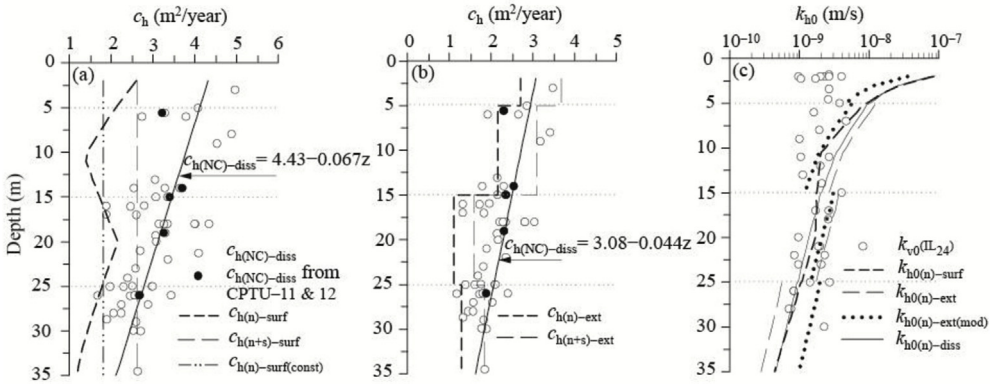

Fig. 11. Coefficients of consolidation and permeability (E-3): (a) and (b) c_h obtained from the surface and extensometer data, respectively, and (c) coefficient of permeability.

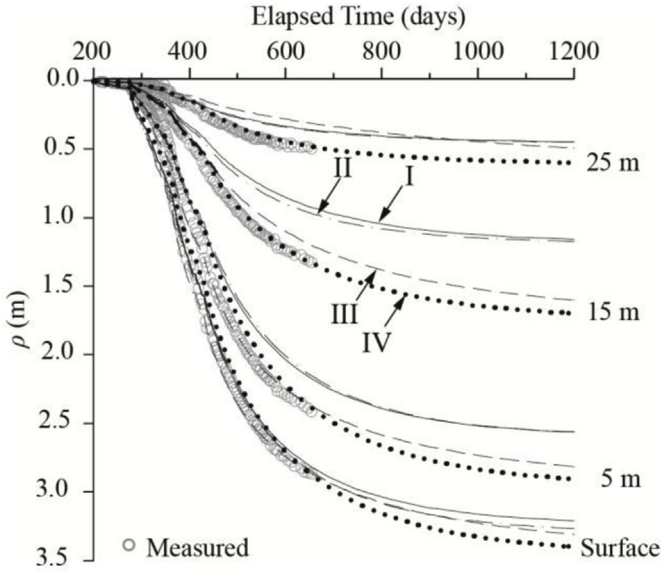

Fig. 13. Comparison of the measured and calculated settlements at location E-3.

Table 4
ρ_{100} obtained using the observational method and FEA at location E-3.

Layer	$\rho_{100(obs)}$	ρ_{fm}	$\rho_{100(FE\text{-}surf)}$ (Cases I to II)	$\rho_{100(FE\text{-}ext)}$ (Cases III to IV)
	(m)	(m)	(m)	(m)
Surface	3.204	2.779	3.290	3.460
0–5	0.425	0.391	0.701	0.493
5–15	1.135	1.062	1.405	1.216
15–25	1.075	0.850	0.727	1.135
25–35	0.551	0.476	0.456	0.616
Σ(ρ of sublayers)	3.186	2.779	3.289	3.460

Note: $\rho_{100(obs)}$ includes the settlement that occurred prior to the measurement (case-III).

obtained using the Asaoka and hyperbolic methods, respectively, which were influenced by ρ_{100} (Table 1).

The consolidation coefficients $c_{h(n)}$ (or $c_{h(n+s)}$) obtained using the surface settlement data and $c_{h(n)\text{-}ext}$ from the extensometer data (location E-3) were compared with the $c_{h(NC)\text{-}diss}$ from the piezocone dissipation tests (Fig. 11a and b). The first result remained constant along the depth, whereas the latter two results varied with depth. A $c_{h(NC)\text{-}diss}$ profile was approximately estimated based on the CPTU-11 and CPTu-12 profiles, which were adjacent to E-3. The estimated $c_{h(NC)}$ profiles should be at least higher than those of $c_{h(n+s)}$ for both cases. Thus, the coefficients of horizontal permeability that correspond to the two settlement data were back-analyzed to vary with CPTU data.

On the basis of the ratio between $c_{h(NC)\text{-}diss}$ and $c_{h(n)}$, $R_c = F/F_n = 1.45$ and 1.80 for the surface settlement and extensometer data, respectively [see Eq. (18)]. This result implies that the settlement curve under the ideal condition (F_n) is identical to the curve that considers the effects of smear and well resistance (F). The $c_{h(n)\text{-}surf}$ and $k_{h0(n)\text{-}surf}$ obtained using surface settlement gauges were adjusted to vary with e_0 under the same R_c value. Fig. 11c shows that the $k_{h0(n)\text{-}surf}$ profile varies in a manner similar to those of $k_{h0(n)\text{-}diss}$ and the coefficient of vertical permeability ($k_{v0(IL24)}$) from the oedometer consolidation tests rather than $k_{h0(n)\text{-}ext}$ from the extensometers.

5. FE analysis

5.1. Modeling and input parameters

The finite element code PLAXIS (2D, Version 8) was used to investigate the validation of the back-analyzed results. The effect of reinforcement obtained from the PVD and sand blanket was disregarded in this analysis (Cao et al., 2016; Fagundes et al., 2017; Han et al., 2017; Jiang et al., 2016; King et al., 2017; Shen et al., 2017; Olsen, 1998; van Eekelen and Brugman, 2016; van Eekelen et al., 2017; Zhang et al., 2016). The E-3 case was typically modeled as a unit cell with an ideal condition (i.e., without smear and well resistance). Then, an axisymmetric analysis was conducted. Fig. 12 shows the meshes (total of 1808) and boundary conditions used in the study. Impermeable and permeable boundaries were applied along the drain to simulate the drainage conditions prior to and after the installation of the PVD (for a period of 250–280 days), respectively. A series of pressures was applied to the top surface according to the same construction timeline. The soft soil material (Stolle et al., 1999; Vermeer and Neher, 1999) was considered for clay. A total of 45 sublayers (at intervals of 1 m) were used to consider variations in material parameters (Fig. 8 – 10, and 12), in which parameters, such as λ^* (= $CR/2.3$) and κ^* (= 2RR/2.3), were calculated using back-analyzed CR and RR, respectively. The permeability coefficient k_h was considered to decrease with a change in the void ratio as follows:

$$\log\left(\frac{k_h}{k_{h0}}\right) = \frac{\Delta e}{C_k} \tag{20}$$

where Δe is the change in void ratio and C_k is the permeability change index. $C_k = 0.5e_0$ was used in this study (Tavenas et al., 1983). A series of four FE analyses for location E-3, namely, Case I for constant CR and RR values; Cases II and III for varying values obtained from surface gauges and extensometers, respectively; and Case IV for the modified

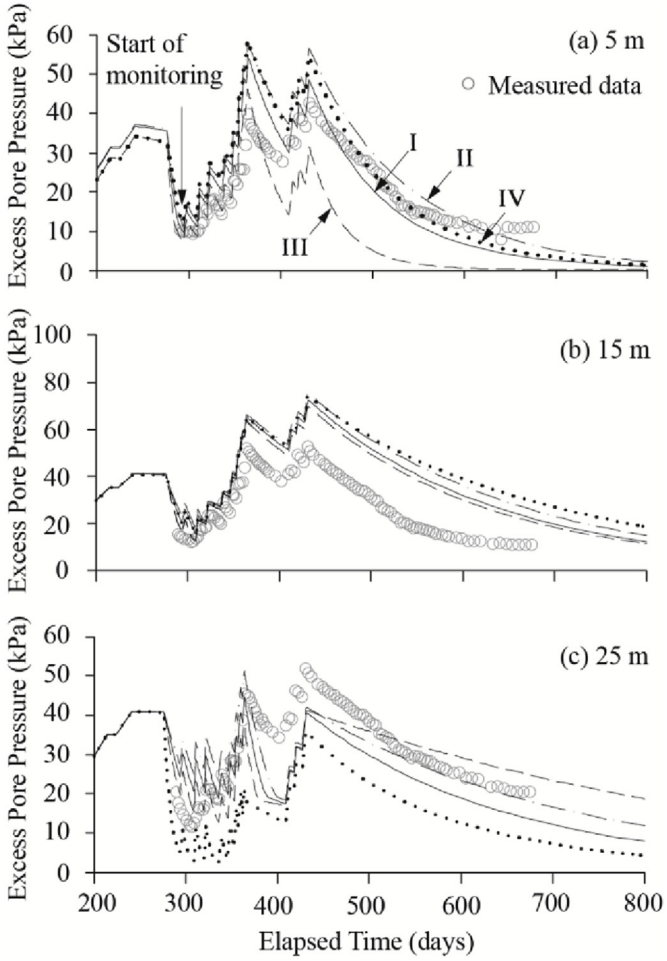

Fig. 14. Comparison of the measured and calculated excess pore pressures (E-3).

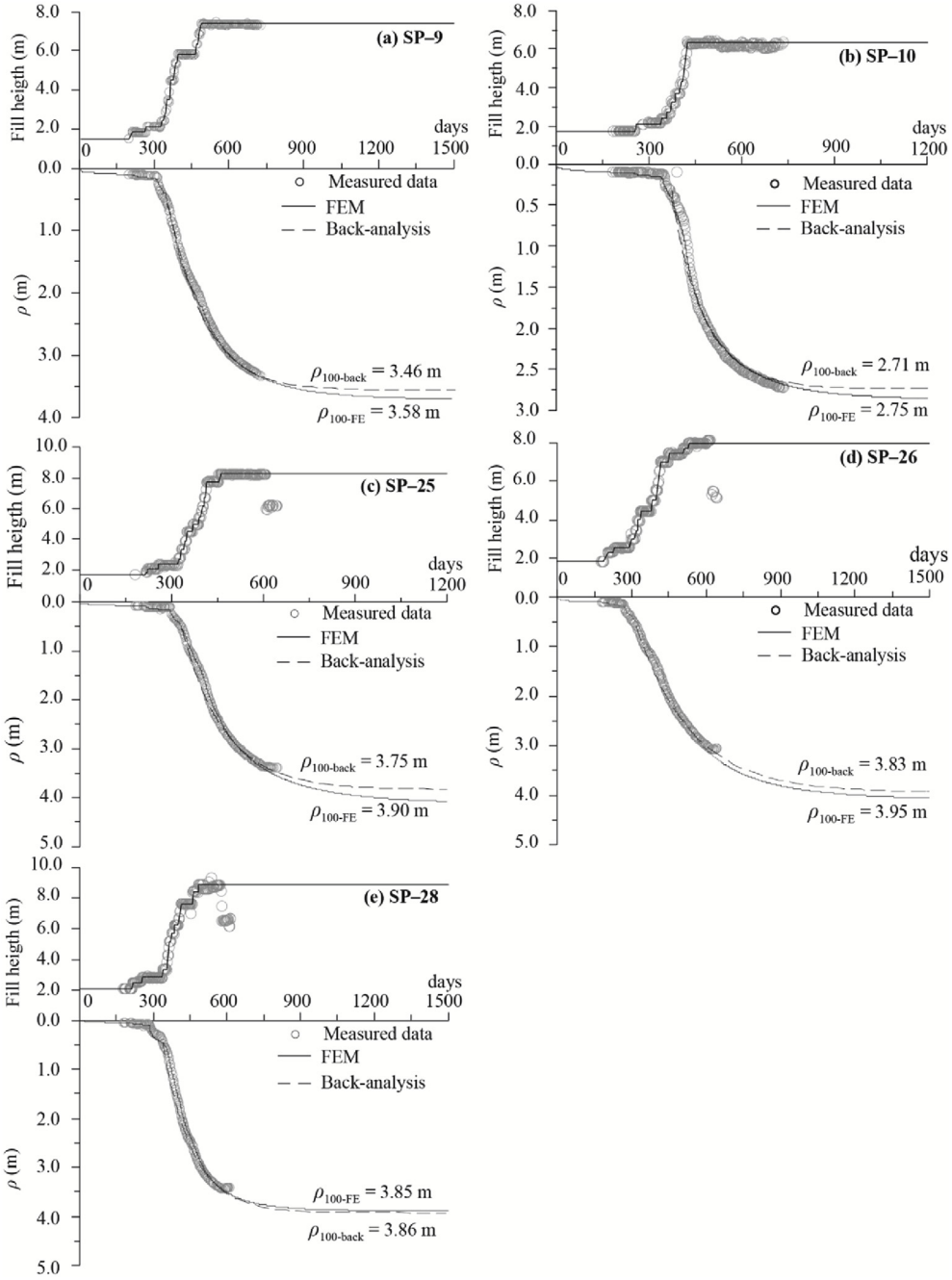

Fig. 15. Comparison of the measured and FE-calculated settlement behaviors at five locations.

$k_{h0(n)}$ in Case III; was performed with different *CR* (or *RR*) and $k_{h0(n)}$ values (Table 3).

5.2. Analyzed results in sublayers

The FE-analyzed settlements for the four cases were compared with the measured settlements at location E-3 (Fig. 13). The FE-based ρ-*t* curves for Cases I to III appeared to agree with the measured surface (or total) settlement behavior. However, such trend was not observed for each sublayer. Cases I and II (based on surface data) exhibited nearly the same behaviors for each sublayer, thereby underestimating the measured behaviors. By contrast, Case III (based on subsurface data) produced a better prediction than the previous ones. The ultimate settlements of each sublayer were compared with one another to determine the cause of their difference (Table 4). $\rho_{100(obs)}$ (= 3.204 m), which was obtained using the surface settlement gauge, was nearly identical to the sum (= 3.186 m) of each ultimate settlement obtained using extensometer data (Table 4). The total settlements were nearly equal to the surface data-based FE result ($\rho_{100(FE\text{-}surf)}$ = 3.29 m) and slightly lower than those of the extensometer-based result ($\rho_{100(FE\text{-}ext)}$ = 3.46 m). Similarly, the $\rho_{100(obs)}$ obtained for each sublayer was close to $\rho_{100(FE\text{-}ext)}$ (Case III). The slight difference between the FE results is attributed to the differently evaluated C_c values (Fig. 8b). Therefore, the behavior differences may be caused mainly by the underestimated $k_{h0(n)}$ rather than by C_c. Fig. 11c shows that a remarkable prediction can be obtained by modifying $k_{h0(n)\text{-}ext}$ to $k_{h0(n)\text{-}ext(mod)}$ (Case IV). Consequently, the newly analyzed ρ-*t* behaviors for each sublayer agreed with the measured behaviors. However, the new result indicated that the effect of well resistance is nearly negligible: $F = R_c F_n = 1.47 \times 2.42 = 3.56$ with $R_c = 1.47$ (Table 3); $F_r = 0.077$

when $F_n = 2.42$ and $F_s = 1.06$ (Table 2).

Fig. 14 shows that the measured and predicted excess pore pressures u_e varied according to construction steps. However, the predicted u_e values exhibited a different trend from the time-settlement behaviors. At a depth of 5 m, the results of Cases I, II, and IV agreed with the measured behavior. Among the three cases, Case III produced the worst prediction. All the predictions made at the following two depths were relatively poor. The modified $k_{h0(n)}$ (Case IV) did not affect the improved prediction of u_e. A better prediction can be possibly obtained by increasing and decreasing $k_{h0(n)}$ at depths of 15 m and 25 m, respectively. Such mismatches may be affected by several factors, including the evaluated geotechnical properties, soil heterogeneity, measured data accuracy, and the location of the piezometers that departed from the center of grouped drains. A number of similar results have also been reported from case studies (Cao et al., 2001; Chai et al., 2001, 2011; Indraratna et al., 2012). An acceptable prediction of settlement and excess pore pressure in the sublayers is difficult to make based on the analyzed results in Figs. 8 and 13−14. Therefore, a large number of subsurface instruments (i.e., small intervals) in a thick clay deposit are required to reliably represent the consolidation behaviors of sublayers and to reevaluate geotechnical properties.

5.3. Total consolidation behaviors

The insufficient information that was obtained from the large intervals of subsurface instruments resulted in the utilization of surface settlement data. First, the validation of the previously back-analyzed geotechnical properties ($c_{h(n)}$ and ρ_{100}), in which the values obtained using the surface settlement data at the other five locations were used (Table 2), should be theoretically verified. A theoretical ρ-t relationship can be obtained by substituting the estimated values into Eq. (21):

$$U_h = \frac{\rho - \rho_0}{\rho_{100} - \rho_0} = \left[1 - \exp\left(-\frac{8}{F_n}\frac{c_{h(n)}t}{d_e^2}\right)\right] \quad (21)$$

Fig. 15 shows that all the theoretical ρ-t curves agree with the measured curves of the locations. Thus, the back-analyzed values are appropriate for representing total settlement behaviors.

The same methods for estimating C_c (or C_r) and $k_{h0(n)}$ (Case II) were adopted. Moreover, FE analysis was conducted for the five locations. Fig. 15 shows that all the FE-analyzed ρ-t curves also agree with the measured and theoretical consolidation behaviors. However, $\rho_{100(FE\text{-}surf)}$ values that were slightly higher than the measurement-based values (ρ_{100}) were observed at three locations. As previously indicated, such difference was unavoidable. Thus, the FE results support the theoretical results. The use of the back-analyzed values with the surface settlement data is sufficient for predicting the total consolidation behavior based on both analyses.

6. Conclusions

We back-analyzed the performance of PVD-improved ground at a site in the Mekong Delta using observational methods. The reevaluated geotechnical parameters based on the analyzed results were compared with those of the laboratory and field soil tests. We conducted FE analysis by using a unit cell model to validate the back-analyzed results. The significant results obtained from the application and the comparisons are as follows.

The beginning and end (ρ_0 and ρ_{100}) of the consolidation settlements were determined using a modified form of the 2D consolidation solution (or an exponential model), and then $c_{h(n)}$ was estimated. The estimated ρ_{ult} (or ρ_{100}) was slightly higher than that of the Asaoka method but significantly lower than that of the hyperbolic method. The σ'_p based on field measurement was higher than that based on the oedometer tests. The compression and recompression indexes were assumed to vary with the in situ void ratio, in which the values obtained using the surface settlement data were within the upper bound of the laboratory values. However, these indexes differed from those of the extensometers. The underestimation of the laboratory test results may be attributed to the poor quality of the samples.

The back-analyzed consolidation behaviors were verified by substituting the estimated ρ_{ult} (or ρ_{100}) and $c_{h(n)}$ into a theoretical consolidation solution. In addition, FE analysis was performed using the reevaluated geotechnical parameters, in which the reevaluated $c_{h(n)}$ was converted to k_{h0} based on an empirical formula. The ultimate settlements of the total layer and sublayers obtained using the observational and FE methods were nearly identical. The FE-based ρ-t curves agreed with the measured surface (or total) settlement behavior. However, such trend was not observed for each sublayer. An excellent prediction of the ρ-t relationships can be possibly obtained by modifying each $k_{h0(n)}$. However, the variations in excess pore pressure were not quantitatively predictable. Accordingly, surface settlement data are sufficient to predict the total consolidation behavior. However, a large number of subsurface instruments are required in thick clay deposits to reliably reevaluate geotechnical properties.

Acknowledgements

This research was supported by Basic Science Research Programs through the National Research Foundation of Korea funded by the Ministry of Science, ICT, and Future Planning (NRF-2016R1A2A2A05005131) and by the Ministry of Education (No. 2016R1A6A1A03012812) and also with the assistance of the graduate students at Dong-A University, Busan, Korea.

References

Asaoka, A., 1978. Observational procedure of settlement prediction. Soils Found. 18 (4), 87–101.
Arulrajah, A., Nikraz, H., Bo, M.W., 2004. Factors affecting field instrumentation assessment of marine lay treated with prefabricated vertical drains. Geotext. Geomembranes 22 (5), 415–437.
Baligh, M.M., Levadoux, J.N., 1986. Consolidation after undrained piezocone penetration, II: Interpretation. J. Geotech. Eng., ASCE 112 (7), 727–745.
Bartlett, S.F., Alcorn, P., 2004. Estimation of Preconsolidation Stress and Compression Ratio from Field and Laboratory Measurements from the I-15 Reconstruction Project, Salt Lake City, Utah. Utah Department of Transportation-Research Division, Salt Lake City Report No. UT-03.20.
Bergado, D.T., Balasubramanian, A.S., Fannin, R.J., Holtz, R.D., 2002. Prefabricated vertical drain (PVD) in soft Bangkok clay: a case of NBIA project. Can. Geotech. J. 39, 304–315.
Bergado, D.T., Enriquez, A.S., Sampaco, C.L., Alfaro, M.C., Balasubramaniam, A.S., 1992. Inversed analysis of geotechnical parameters on improved soft Bangkok clay. J. Geotech. Geoenviron. Eng., ASCE 118 (7), 1012–1030.
Bergado, D.T., Mukherjee, K., Alfaro, M.C., Balasubramaniam, A.S., 1993. Prediction of vertical-band-drain performance by the finite-element method. Geotext. Geomembranes 12 (6), 567–586.
Bergado, D.T., Long, P.V., Balasubramanian, A.S., 1996. Compressibility and flow parameters from PVD improved soft Bangkok clay. Geotech. Eng. 27 (2), 1–20.
Bo, M.W., Chu, J., Low, B.K., Choa, V., 2003. Soil Improvement: Prefabricated Vertical Drain Techniques. Thomson, Singapore, pp. 341.
Cao, L.F., Chang, M.F., Teh, C.I., Na, Y.M., 2001. Back-calculation of consolidation parameters from field measurements at a reclamation site. Can. Geotech. J. 38 (4), 755–769.
Cao, W.Z., Zheng, J.J., Zhang, J., Zhang, R.J., 2016. Field test of a geogrid-reinforced and floating pile-supported embankment. Geosynth. Int. 23 (5), 348–361.
Chai, J.C., Shen, S.L., Miura, N., Bergado, D.T., 2001. Simple method of modeling PVD improved subsoil. J. Geotech. Geoenviron. Eng., ASCE 127 (11), 965–972.
Chai, J.C., Bergado, D.T., Shen, S.L., 2011. Modelling prefabricated vertical drain improved ground in plane strain analysis. Proc. Inst. Civ. Eng. Ground Improv. 166 (2), 65–77.
Chu, J., Bo, M.W., Choa, V., 2006. Improvement of ultra-soft soil using prefabricated vertical drains. Geotext. Geomembranes 24 (6), 339–348.
Chung, S.G., 1999. Engineering properties and consolidation characteristics of Kimhae estuarine clayey soil. In: Thick Deltaic Deposits, ATC-7 Workshop, Special Publication, the 11th ARC on SMGE, Seoul, pp. 93–108.
Chung, S.G., Kweon, H.J., Jang, W.Y., 2014a. A hyperbolic fit method for interpretation of piezocone dissipation tests. J. Geotech. Geoenviron. Eng., ASCE 140 (1), 251–254.
Chung, S.G., Kweon, H.J., Jang, W.Y., 2014b. Observational method for field performance of prefabricated vertical drains. Geotext. Geomembranes 42 (4), 405–416.
Chung, S.G., Lee, N.K., 2010. Smear effect and well resistance of PVD-installed ground based on the hyperbolic method. J. Geotech. Geoenviron. Eng. ASCE 136 (4),

640–642.
Chung, S.G., Lee, N.K., Kim, S.R., 2009. Hyperbolic method for prediction of prefabricated vertical drains performance. J. Geotech. Geoenviron. Eng. ASCE 135 (10), 1519–1528.
Debats, J.M., Scharff, G., Balderas, J., Melentijevic, S., 2013. Ground improvement efficiency and back-analysis of settlements. Proc. Inst. Civ. Eng. Ground Improv. 166 (3), 138–154.
Edil, T.B., Fox, P.J., Lan, L.T., 1991. Observational procedure for settlement of peat. In: Proc. Of the Int. Conf. on Geotechnical Engineering for Coastal Development Theory and Practice on Soft Ground, pp. 165–170 Geo-Coast'91, Yokohama, Japan.
Fagundes, D.F., Almeida, M.S.S., Thorel, L., Blanc, M., 2017. Load transfer mechanism and deformation of reinforced piled embankments. Geotext. Geomembranes 45 (2), 1–10.
Han, J., Wang, F., Al-Naddaf, M., Xu, C., 2017. Progressive development of two-dimensional soil arching with displacement. Int. J. GeoMech. 17 (12), 04017112.
Hawlader, B.C., Imai, G., Muhunthan, B., 2002. Numerical study of the factors affecting the consolidation of clay with vertical drains. Geotext. Geomembranes 20 (4), 213–239.
Indraratna, B., Rujikiatkamjorn, C., Balasubramaniam, A.S., McIntosh, G., 2012. Soft ground improvement via vertical drains and vacuum assisted preloading. Geotext. Geomembranes 30, 16–23.
Jang, W.Y., Chung, S.G., 2014. Long-term settlement analysis of partially improved thick clay deposit. Geotext. Geomembranes 42 (6), 620–628.
Jiang, Y., Han, J., Parsons, R.L., Brennan, J.J., 2016. Field instrumentation and evaluation of modular-block MSE walls with secondary geogrid layers. J. Geotech. Geoenviron. Eng. 142 (12), 05016002.
Karim, M.R., Manivannan, G., Gnanendran, C.T., Lo, S.-C.R., 2011. Predicting the long-term performance of a geogrid-reinforced embankment on soft soil using two-dimensional finite element analysis. Can. Geotech. J. 48 (5), 741–753.
King, D.J., Bouazza, A., Gniel, J.R., Rowe, R.K., Bui, H.H., 2017. Serviceability design for geosynthetic reinforced column supported embankments. Geotext. Geomembranes 45 (4), 261–279.
Kulhawy, F.H., Mayne, P.W., 1990. Manual on Estimating Soil Properties for Foundation Design. Report EPRI EL-6800. Electric Power Research Institute, Palo Alto. Calif, pp. 306.
Lam, L.G., Bergado, D.T., Hino, T., 2015. PVD omprovement of soft Bangkok clay with and without vacuum preloading using analytical and numerical analyses. Geotext. Geomembranes 43 (6), 547–557.
Lee, N.K., Chung, S.G., 2010. Reevaluation of the factors influencing the consolidation of ground by incorporating prefabricated vertical drains. KSCE J. Civ. Eng. 14 (2), 155–164.
Leroueil, S., Magnan, J.P., Tavenas, F., 1990. Embankments on Soft Clays. Ellis Horwood, London, pp. 360.
Leroueil, S., Tavenas, F., Samson, L., Morin, P., 1983. Preconsolidation pressure of Champlain clays. Part II. Laboratory determination. Can. Geotech. J. 20 (4), 803–816.
Leroueil, S., Tavenas, F., Mieussens, C., Peignaud, M., 1978. Construction pore pressures in clay foundations under embankments, Part 2: generalized behavior. Can. Geotech. J. 15 (1), 66–82.
Liu, H.L., Chu, J., 2009. A new type of prefabricated vertical drain with improved properties. Geotext. Geomembranes 27 (2), 152–155.
Lo, S.R., Mak, J., Gnanendran, C.T., Zhang, R., Manivannan, G., 2008. Long-term performance of a wide embankment on soft clay improved with prefabricated vertical drains. Can. Geotech. J. 45 (8), 1073–1091.
Magnan, J.P., Pilot, G., Queyroi, D., 1983. Back analysis of soil consolidation around vertical drains. In: 8th ECSMFE, vol. 2. Balkema, Helsinki, pp. 653–658.
Morin, P., Leroueil, S., Samson, L., 1983. Preconsolidation pressure of Champlain clays. Part I. In-situ determination. Can. Geotech. J. 20 (4), 782–802.
Nguyen, V.L., Ta, T.K.O., Tateishi, M., 2000. Late Holocene depositional environments and coastal evolution of the Mekong River delta, southern Vietnam. J. Asian Earth Sci. 18 (4), 427–439.
Nguyen, V.L., Ta, T.K.O., Tateishi, M., Kobayashi, I., Umitsu, M., Saito, Y., 2005. Late quaternary depositional sequences in the Mekong river delta, Vietnam. In: Chen, Z., Yoshiki, S., Goodbred, S.L. (Eds.), Mega-deltas of Asia: Geological Evolution and Human Impact. Ocean Press, Beijing, pp. 121–127.
Olsen, R.E., 1998. 31st Terzaghi Lecture: settlement of embankments on soft clays. J. Geotech. Geoenviron. Eng. 124 (4), 278–296.
Rezania, M., Bagheri, M., Nezhad, M.M., Sivasithamparam, N., 2017. Creep analysis of an earth embankment on soft soil deposit with and without PVD improvement. Geotext. Geomembranes 45 (5), 537–547.
Rowe, R.K., Taechakumthorn, C., 2008. Combined effect of PVDs and reinforcement on embankments over rate-sensitive soils. Geotext. Geomembranes 26 (3), 239–249.
Rujikiatkamjorn, C., Indraratna, B., 2015. Analytical solution for radial consolidation considering soil structure characteristics. Can. Geotech. J. 52 (7), 947–960.
Saowapakpiboon, J., Bergado, D.T., Voottipruex, P., Lam, L.G., Nakakuma, K., 2011. PVD improvement combined with surcharge and vacuum preloading including simulations. Geotext. Geomembranes 29 (1), 74–82.
Shen, P., Xu, C., Han, J., 2017. Model tests investigating spatial tensile behavior of simulated geosynthetic reinforcement material over rigid supports. J. Mater. Civ. Eng. 30 (2), 04017288.
Skempton, A.W., 1944. Notes on the compressibility of clays. Q. J. Geol. Soc. Lond. 100, 119–135.
Singh, V.K., Chung, S.G., 2015. Correlations of the overconsolidation ratios between laboratory and in situ tests on Busan clay. Eng. Geol. 199, 38–47.
Stolle, D.F.E., Vermeer, P.A., Bonnier, P.G., 1999. Consolidation model for a creeping clay. Can. Geotech. J. 36 (4), 754–759.
Ta, T.K.O., Nguyen, V.L., Tateishi, M., Kobayashi, I., Tanabe, S., Saito, Y., 2002. Holocene delta evolution and sediment discharge of the Mekong River, southern Vietnam. Quat. Sci. Rev. 21 (16−17), 1807–1819.
Taechakumthorn, C., Rowe, R.K., 2012. Performance of a reinforced embankment on a sensitive Champlain clay deposit. Can. Geotech. J. 49 (8), 917–927.
Tan, T.S., Inoue, T., Lee, S.L., 1991. Hyperbolic method for consolidation analysis. J. Geotech. Geoenviron. Eng. ASCE 117 (11), 1723–1737.
Tanaka, H., 2002. Reevaluation of established relations between index properties and soil parameters. In: In: Nakase, A., Tsuchida, T. (Eds.), Proc. The Intl. Symp. (IS-Yokohama), Coastal Geotechnical Engineering in Practice, vol. 2. Balkema Pub., Lisse, pp. 3–26.
Tavenas, F., Jean, P., Leblond, P., Leroueil, S., 1983. The permeability of natural soft clays, part II: permeability characteristics. Can. Geotech. J. 20 (4), 645–660.
van Eekelen, S.J.M., Brugman, M.H.A., 2016. Design Guideline Basal Reinforced Piled Embankments. SBRCURnet and CRC Press, Delft, Netherlands.
van Eekelen, S.J.M., Venmans, A.A.M., Bezuijen, A., van Tol, A.F., 2017. Long term measurements in the Woerden geosynthetic-reinforced pile-supported embankment. Geosynth. Int. 1–15. https://doi.org/10.1680/jgein.17.00022.
Vermeer, P.A., Neher, H.P., 1999. A soft soil model that accounts for creep. In: Brinkgreve, R.B.J. (Ed.), Beyond 2000 in Computational Geotechnics - 10 Years of Plaxis International. Balkema, Rotterdam, pp. 249–261.
Voottipruex, P., Bergado, D.T., Lam, L.G., 2014. Back-analyses of flow parameters of PVD improved soft Bangkok clay with and without vacuum preloading from settlement data and numerical simulations. Geotext. Geomembranes 42 (5), 457–467.
Watabe, Y., Leroueil, S., 2015. Modelling and implementation of the isotache concept for long-term consolidation behavior. Int. J. Geotech. 15 (5) A4014006–1−8.
Zhang, C., Jiang, G., Liu, X., Buzzi, O., 2016. Arching in geogrid-reinforced pile-supported embankments over silty clay of medium compressibility: field data and analytical solution. Comput. Geotech. 77, 11–25 July.

Notations

$\bar{B}$: ratio of excess pore pressure to applied pressure
C_c: compression index
$C_{c(back)}$: back-analyzed compression index
C_{c1}: initial virgin compression index
C_{c2}: second virgin compression index
C_k: change index of permeability
C_r: recompression index
$C_{r(back)}$: back-analyzed recompression index
c_h: coefficient of horizontal consolidation
$c_{h(NC)\text{-}diss}$: coefficient of horizontal consolidation in the NC domain, which is obtained from piezocone dissipation test
$c_{h(n)}$: coefficient of horizontal consolidation for an ideal condition
$c_{h(n),ave}$: the average value of $c_{h(n)}$
$c_{h(n)\text{-}ext}$: $c_{h(n)}$ obtained using extensometers data
$c_{h(n)\text{-}surf}$: $c_{h(n)}$ obtained using surface gauge data
$c_{h(n)\text{-}var}$: time-dependent $c_{h(n)}$
$c_{h(n+s)}$: coefficient of horizontal consolidation with the spacing and smear effects
$c_{h(n+s)\text{-}ext}$: $c_{h(n+s)}$ obtained using extensometer data
$c_{h(OC)\text{-}diss}$: coefficient of horizontal consolidation obtained from the piezocone dissipation test
CR: compression ratio
d_e: diameter of influence zone of each drain
d_m: equivalent diameter of mandrel
d_s: equivalent diameter of smear zone
d_w: equivalent diameter of drain
e_0: initial void ratio
F: factor = $F_n + F_s + F_r$
F_n: factor to account for drain spacing
F_r: factor to account for well resistance
F_s: factor to account for smear effect
$F_{(n+s)}$: factor to account for drain spacing and smear effect
H_{cr}: critical height
h_w: incremental water height due to the fill placement
I_L: liquidity index
$k_{v0(IL24)}$: initial vertical permeability coefficient obtained from oedomter test (IL_{24})
k_h: horizontal permeability coefficient
$k_{h0\text{-}back}$: back-analyzed horizontal permeability coefficient
$k_{h0\text{-}diss}$: coefficient of horizontal permeability obtained from the piezocone dissipation test
$k_{h0(n)}$: coefficient of horizontal permeability for an ideal condition
$k_{h0(n)\text{-}ext}$: coefficient of horizontal permeability obtained using extensometers data for an ideal condition
$k_{h0(n)\text{-}ext(mod)}$: modified $k_{h0(n)\text{-}ext}$
$k_{h0(n)\text{-}surf}$: $k_{h0(n)}$ obtained using surface settlement data
k_s: coefficient of horizontal permeability in smear zone
L: thickness of clay
m: total number of soil layers
n: drain spacing ratio = d_e/d_w
q_t: corrected cone tip resistance
R_c: F_n / F or $c_{h(n)} / c_h$
RR: recompression ratio
s: spacing of drains
$s_{u,FV}$: undrained shear strength from field van shear test
t: time
t_0: time at the initiating of the primary consolidation
T_h: time factor

$T_{h(n)}$: time factor to account for drain spacing (ideal condition)
u_e: excess pore pressure
u_2: pore pressure measured at the shoulder of cone
U_h: degree of horizontal consolidation
w_L: liquid limit
w_n: water content
w_p: plastic limit
γ_t: total unit weight of soil
γ_w: unit weight of water
Δe: change in void ratio
Δh: thickness of each sublayer
Δt: time interval
Δu: excess pore pressure increment
$\Delta\gamma$: difference between the saturated and bulk unit weights
$\Delta\sigma$: stress increment
$\Delta\sigma_{cr}$: the incremental stress due to the critical fill height H_{cr}
$\Delta\sigma_v$: applied pressure increment
$\dot{\varepsilon}_f$: finally measured strain rate
α: intercept of a straight line in t/ρ vs. t plot
β: slope of a straight line in t/ρ vs. t plot
β_0: intercept of a straight line in ρ_i vs. ρ_{i-1} plot
β_1: slope of a straight line in ρ_i vs. ρ_{i-1} plot
η: exponent
κ: coefficient
λ: empirical ratio
κ^*: modified recompression index
λ^*: modified compression index
ρ: settlement
ρ_c: consolidation settlement
ρ_m: finally measured settlement
ρ_r: recompression settlement
ρ_0: initial settlement of consolidation settlement
ρ_{100} (ρ_{ult}): ultimate settlement
$\rho_{100(FE\text{-}ext)}$: ultimate settlement obtained from FE-analysis using the extensometer data
$\rho_{100(FE\text{-}surf)}$: ultimate settlement obtained from FE-analysis using the surface settlement data
$\rho_{100(obs)}$: ρ_{100} includes the settlement that occurred prior to the measurement
σ'_p: preconsolidation stress
σ'_{v0}: effective overburden stress
σ_{v0}: total overburden stress
Φ: coefficient $= \frac{\ln(1-U_h)}{\ln\left(1-U_{exp}^{1/\kappa}\right)}$